Terr. Atmos. Ocean. Sci., Vol. 20, No. 5, 671-685, October 2009 doi: 10.3319/TAO.2008.10.13.01(T)

Scaled Energies of M_L 5.1 Aftershocks of the 1999 Chi-Chi, Taiwan, Earthquake Measured from Local Seismograms

Ming-Wey Huang[1, 2, *] and Jeen-Hwa Wang[2]

[1] *National Science and Technology Center for Disaster Reduction, Taipei 231, Taiwan, ROC*
[2] *Institute of Earth Sciences, Academia Sinica, Taipei, Taiwan, ROC*

Received 28 May 2008, accepted 13 October 2008

ABSTRACT

In this study, we measure the seismic radiation energy, E_s, and seismic moment, M_o, of twenty-two larger-sized aftershocks with 5.1 M_L 6.5 of the 1999 M_s 7.6 Chi-Chi, Taiwan, earthquake from high-quality digital strong-motion data recorded at stations with epicentral distances of less than 50 km through a method proposed by Andrews (1986). We also eliminate the effects on the measures of E_s and M_o due to site amplification and finite frequency bandwidth limitation. Comparison of the values of M_o obtained in this study and those listed in the Harvard CMT catalogue shows that Andrews' method to measure M_o from local seismograms is acceptable. The measured values are $E_s = 2.0$ $10^{18} - 8.9$ 10^{21} g cm^2 sec^{-2} and $M_o = 1.3$ $10^{23} - 1.4$ 10^{26} g cm sec^{-2} cm^{-1}, which give the scaled energy to be $E_s/M_o = 7.4$ $10^{-6} - 2.6$ 10^{-4}. The scaled energies of the 22 events are dependent upon earthquake magnitude, M_s, when both E_s and M_o are evaluated from local seismograms; yet, independent of M_s when M_o is estimated from teleseismic data. Scaled energy slightly depends on the depth, h (in km), through the following form: $E_s/M_o = 1.92$ $10^{-5} e^{0.09h}$. In addition, the corner frequency, f_c, is also measured. Its value ranges from 0.15 to 1.34. The scaling law between M_o and f_c is: $M_o \sim f_c^{-3.65}$.

Key words: Scaled energy, Radiation energy, Seismic moment, Aftershocks, Chi-Chi earthquake

Citation: Huang, M. W. and J. H. Wang, 2009: Scaled energies of M_L 5.1 aftershocks of the 1999 Chi-Chi, Taiwan, earthquake measured from local seismograms. Terr. Atmos. Ocean. Sci., 20, 671-685, doi: 10.3319/TAO.2008.10.13.01(T)

1. INTRODUCTION

The seismic-wave energy, E_s, and seismic moment, M_o, are two commonly used parameters quantifying earthquakes and can be directly measured from seismograms. The scaled energy, E_s/M_o, which is defined to be the ratio of seismic radiation energy to seismic moment, denotes the radiated energy per unit seismic moment of an earthquake. Several factors could affect the measures of E_s and M_o from local, regional, and teleseismic data, thus, resulting in high divergence of E_s/M_o (Vassiliou and Kanamori 1982; Kikuchi and Fukao 1988; Choy and Boatwright 1995). Generally, E_s measured from local seismograms is larger than that done from teleseismic data (Bolt 1986; Smith et al. 1991; Singh and Ordaz 1994; Hwang et al. 2001; Huang et al. 2002). The strong site effect at higher frequencies (greater than 0.01 Hz) can produce an overestimation of source parameters (Boatwright et al. 2002; Pérez-Campes et al. 2003) while finite frequency bandwidth limitation leads to an opposite effect (Hwang et al. 2001; Ide and Beroza 2001; Wang 2004). Boore (1988), Di Bona and Rovelli (1988), and Singh and Ordaz (1994) stressed that E_s can be underestimated when high-frequency signals are not included. On the other hand, the estimate of M_o from long-period teleseismic data has lower uncertainty due to the use of longer-period signals.

Kanamori (1977) showed $E_s/M_o = 2$ 10^{-4} for great earthquakes. Vassilion and Kanamori (1982) reported $E_s/M_o = 2$ 10^{-4} for shallow earthquake and 4.6 10^{-5} for deep and intermediate events. Kikuchi and Fukao (1988) stated that the value of E_s/M_o is confined to a narrow range of 10^{-6} - 10^{-5}, with an average of ~5.0 10^{-6}. They also stressed that during an earthquake rupture energy loss due to cohesion cannot be ignored. Brodsky and Kanamori (2001) reported an abrupt increase in E_s/M_o from 10^{-6} to 10^{-4} almost at $M_w = 5$, where M_w is the moment magnitude. Kanamori and Rivera (2004) suggested an increase in E_s/M_o with M_w when M_o relates to corner

* *Corresponding author*
E-mail: mwhuang@ncdr.nat.gov.tw

frequency, f_c, in a form of $M_o \sim f_c^{-(3+\varepsilon)}$ with $\varepsilon > 0$. On the contrary, Ide and Beroza (2001) showed that E_s/M_o is almost a constant of about 3 10^{-5} in a large range of M_w from -4 to 9. For 94 interplate and 74 intraplate earthquakes with M_o = $10^{13} - 10^{18}$ N-m in the Kanto area, Japan recorded by 27 borehole and 7 surface hard-rock stations, Kinoshita and Ohike (2002) reported that $E_s/M_o = (1.15 - 12.9)$ 10^{-5} and is weakly dependent on M_o. Hence, the problem of whether E_s/M_o depends upon earthquake magnitude or not is still open.

The Chi-Chi earthquake of 20 September 1999 ruptured the Chelungpu fault in central Taiwan (Ma et al. 1999; Shin et al. 2000). In addition to the mainshock, a large number of aftershocks were recorded by an island-wide seismic network, including more than 600 free-field strong-motion stations, operated by the Central Weather Bureau (CWB) (Shin et al. 2000). Hwang et al. (2001) measured the values of E_s, M_o, and E_s/M_o of the mainshock from near-fault seismic data. Wang (2004) and Wang and Huang (2007) corrected their value of E_s to remove the effect of finite frequency bandwidth limitation. Huang et al. (2002) measured the scaled energies for two larger-sized aftershocks from local seismograms.

In this study, we attempt to measure E_s and M_o and then to estimate E_s/M_o for twenty-two larger-sized aftershocks with 5.1 M_L 6.8 (CWB 2003), whose epicenters are near the Chi-Chi mainshock and to the east of the Chelungpu fault (see Fig. 1), from local seismograms (with epicentral distances of less than 50 km) using the method proposed by Andrews (1986). The values of E_s and M_o of two aftershocks, which were studied by Huang et al. (2002), are remeasured in this study. Before estimating the source parameters, finite frequency bandwidth limitation and site amplification must be taken into account. Similar to Ide and Beroza (2001), a way of eliminating the effects on the measured values of E_s, and M_o, and E_s/M_o caused by finite frequency bandwidth limitation based on the ω-squared source model will be investigated. However, Ide and Beroza (2001) only considered the effect due to the upper-bound frequency; while in this study the effects caused by low- and upper-bound frequencies are both taken into account. Additionally, the site effect due to near-surface soil strata would amplify or de-amplify the ground motions. This will influence estimates of source parameters (cf. Pérez-Campos et al. 2003). Site amplification of seismic waves is usually a function of frequency, and stronger at a soil site than at a rock one. The seismic stations are commonly built on both the rock and soil sites. Thus, the corrections of seismic-wave amplitudes caused by site amplifications must be done before seismic data are used to estimate source parameters. Finally, the variations of E_s/M_o with earthquake magnitude and depth will be presented and discussed.

2. DATA

The 22 aftershocks in use have M_L = 5.1 - 6.8 and focal depths of 3.6 - 22.1 km. The epicentral distances between the earthquakes and accelerographs are in the range 2 - 45 km. The source parameters of the 22 aftershocks are listed in Table 1. The epicenters of the 22 aftershocks are shown in Fig. 1. Included also in the figure are the fault-plane solutions of 14 events (Kao et al. 2002). Except for one, the remaining 13 events are thrust faulting, with or without a strike-slip component, even though their focal-plane solutions cannot be exactly determined. The surface-wave magnitude, M_s, of ten events listed in the Harvard CMT catalogue are also shown in Table 1.

The strong-motion array operated by the Central Weather Bureau (CWB) consists of more than 600 free-field accelerographs, which are characterized by a flat frequency response from DC to about 50 Hz (Liu et al. 1999). Although there are so many seismic stations, for an event in study only the accelerograms recorded at a small number of seismic stations can be used because of a high triggering level, strong background noise, large site effects, etc. Since most of the strong-motion stations near the earthquakes are situated to the west of their individual epicenters, six stations placed at the eastern boundary of the Central Range are also selected to widen the azimuthal coverage of stations for an event. The stations in use are displayed with solid triangles in Fig. 1. The source parameters of two events, coded Nos. 20 and 21 in Table 1, were estimated by Huang et al. (2002). However, they did not take the effects due to site amplification and finite frequency bandwidth limitation into account. In this study, the source parameters of the two events will be re-estimated. It is noted that the seismic stations used for an event are situated in, at least, two quarters of and not close to either nodal plane of its focal sphere. Hence, the effect due to seismic radiation pattern could be eliminated after averaging.

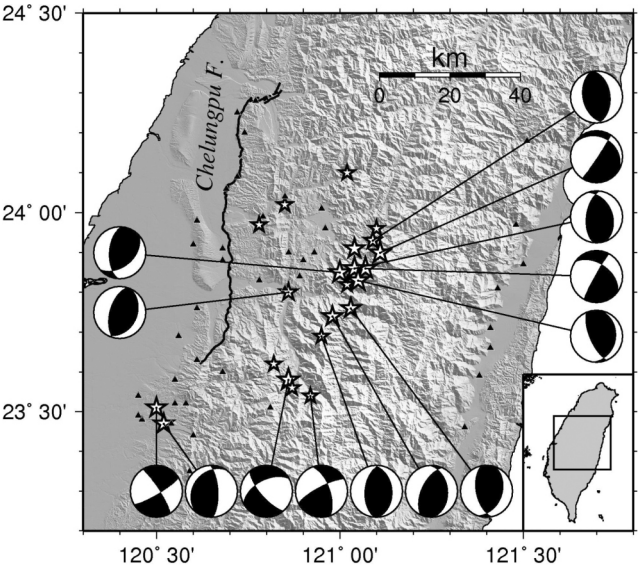

Fig. 1. The epicenters (denoted by solid circles) of 22 aftershocks. Included also are the fault-plane solutions of 12 events.

Table 1. Earthquake parameters of twenty aftershocks in this study.

No.	Events	Long. (°E)	Lat. (°N)	Depth (km)	M_L	M_s	M_o (g cm sec^{-2} cm^{-1})	E_s (g cm^2 sec^{-2})	E_s/M_o	f_c (Hz)
1	199909201757	121.03	23.93	11.0	6.4	(5.9)	2.6×10^{24}	1.1×10^{20}	4.2×10^{-5}	0.47
2	199909201803	120.86	23.80	9.8	6.6	(6.1)*	1.4×10^{26}	8.9×10^{21}	6.4×10^{-5}	0.15
3	199909201811	121.07	23.87	12.5	6.7	(6.2)*	1.9×10^{25}	1.1×10^{21}	5.8×10^{-5}	0.29
4	199909201816	121.04	23.86	12.5	6.7	(6.2)*	3.0×10^{25}	2.7×10^{21}	9.0×10^{-5}	0.29
5	199909201821	121.06	23.96	9.7	5.2	(4.5)	1.5×10^{23}	1.1×10^{19}	7.3×10^{-5}	1.30
6	199909201832	120.99	23.83	16.8	5.1	(4.4)	1.3×10^{23}	2.1×10^{18}	1.6×10^{-5}	0.97
7	199909201940	120.88	23.55	7.4	5.3	(4.6)*	6.8×10^{24}	6.2×10^{20}	9.1×10^{-5}	0.50
8	199909201957	120.81	24.03	12.0	5.2	(4.5)	2.1×10^{23}	3.2×10^{18}	1.5×10^{-5}	0.82
9	199909202002	120.74	23.98	12.1	5.4	(4.7)	4.4×10^{23}	1.6×10^{19}	3.6×10^{-5}	0.79
10	199909202021	120.98	24.11	11.1	5.2	(4.5)	2.7×10^{23}	2.0×10^{18}	7.4×10^{-6}	0.61
11	199909202146	120.86	23.59	8.6	6.6	6.5*	8.1×10^{25}	7.0×10^{21}	8.6×10^{-5}	0.20
12	199909202154	120.77	23.62	4.3	5.3	(4.7)	3.5×10^{24}	1.1×10^{20}	3.1×10^{-5}	0.40
13	199909202222	120.83	23.55	5.0	5.2	(4.5)	3.4×10^{23}	7.6×10^{18}	2.2×10^{-5}	0.72
14	199909220014	121.07	23.83	12.6	6.8	6.4*	5.0×10^{25}	1.0×10^{22}	2.0×10^{-4}	0.30
15	199909220049	121.05	23.74	8.2	6.2	5.9*	1.2×10^{25}	1.3×10^{21}	1.1×10^{-4}	0.38
16	199909221217	121.03	23.76	22.1	6.0	4.9*	1.3×10^{24}	2.1×10^{20}	1.6×10^{-4}	0.97
17	199909231244	121.07	23.95	4.1	5.7	4.8*	1.3×10^{24}	5.8×10^{19}	4.5×10^{-5}	0.62
18	199909250843	121.03	23.72	3.6	5.1	4.8*	1.2×10^{24}	1.6×10^{19}	1.3×10^{-5}	0.44
19	199909252352	121.11	23.84	9.1	6.8	6.4*	5.7×10^{25}	2.4×10^{21}	4.2×10^{-5}	0.20
20	199910220218	120.52	23.51	24.5	6.4	5.6*	2.9×10^{25}	5.1×10^{21}	1.8×10^{-4}	0.36
21	199910220310	120.50	23.90	24.0	6.0	5.3*	1.2×10^{25}	3.1×10^{21}	2.6×10^{-4}	0.49
22	200006101823	121.11	23.90	16.2	6.7	6.2*	2.1×10^{25}	2.0×10^{21}	9.5×10^{-5}	0.31

** from the BATS catalogue.*

The velocity waveforms of two horizontal components are first integrated once from the accelerograms, and then are rotated from the original geographic coordinate system to a system defined based on the ray-path direction between seismic station and hypocenter. In the new system, the radial (R) component vibrates along the ray-path and the transverse component (T) is normal to the R-component. Most of the 22 events and stations in use are located at the Western Foothills, some of them are in the Central Range, and a few of them are in eastern Taiwan. Although the shallow velocity structure varies somewhat uniformly from east to west, the deeper one is relatively more uniform (cf. Ma et al. 1996). Hence, the difference in the physical properties between any two event-station pairs is likely be small and can be ignored in such a small area.

An example of the rotated velocity waveforms for No. 2 Event ($M_L = 6.6$) at 6 stations are shown in Fig. 2. The T- and R-components are displayed on the left-hand side and right-hand side diagrams, respectively. Larger amplitudes can be seen at Stations TCU076 and TCU078. The amplitudes at the other 4 stations are relatively small. The cumulative energies (integral of squared spectral amplitudes of velocities) are shown in Fig. 3, in which the solid and dashed lines represent the T- and R-components, respectively. The cumulative energies increase mainly in the frequency range 0 - 6 Hz, and then become flat when the frequency, f, is greater than 6 Hz. This suggests that the energies radiated mainly in the frequency range 0 - 6 Hz during this earthquake. The energies with $f > 6$ Hz are scattered due to local structures. Thus, we take the upper bound, f_u, of the frequency range to be 6 Hz for data processing.

3. METHOD OF MEASURING E_s AND M_o

The seismic radiation energy, E_s, must be measured from both P- and S-waves (Choy and Boatwright 1995). As shown

in Fig. 2, the *P*-waves, however, cannot be completely recorded by local accelerographs because the recording process is triggered only when the ground motion is larger than a critical level. A lack of *P*-waves would lead to an underestimation of E_s. It is difficult to accurately evaluate measurement error from accelerograms due to incomplete *P*-waves. However, since the *P*-waves are usually several times weaker than the *S*-waves, the error should be small. In this study, we only measure the values of E_s from the *S*-waves. Hence, the measured value of E_s will be slightly less than the real one.

Let $d(t)$ and $v(t)$ be the time functions of displacements and velocities of ground motions. The Fourier transforms of $d(t)$ and $v(t)$ are, respectively, $D(f)$ and $V(f)$. An approximation of $D(f)$ is (Aki 1967; Brune 1970):

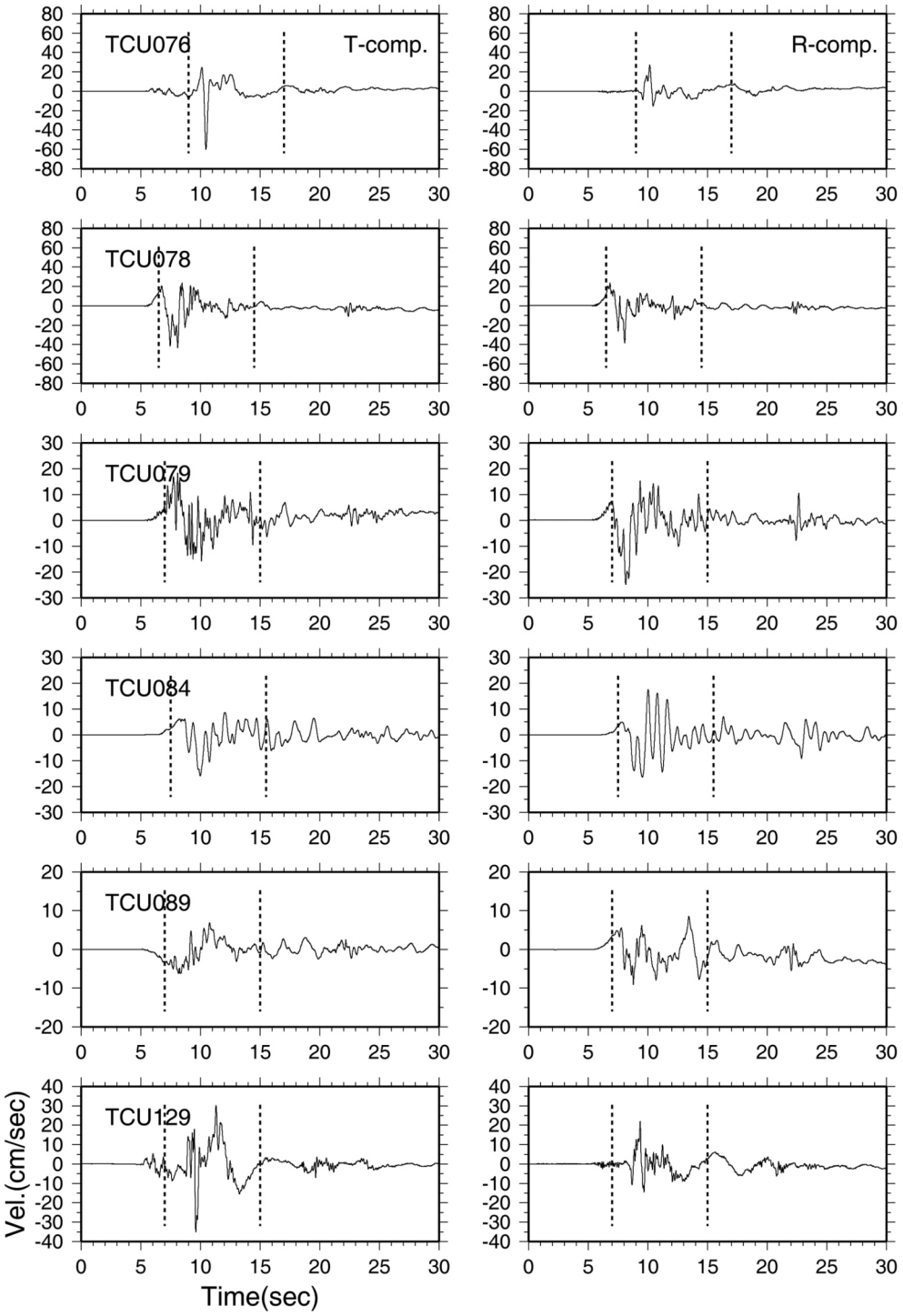

Fig. 2. The *T*- and *R*-component of velocity seismograms at 6 stations in use for the No. 2 event. The two dashed lines depict the *S*-wave train.

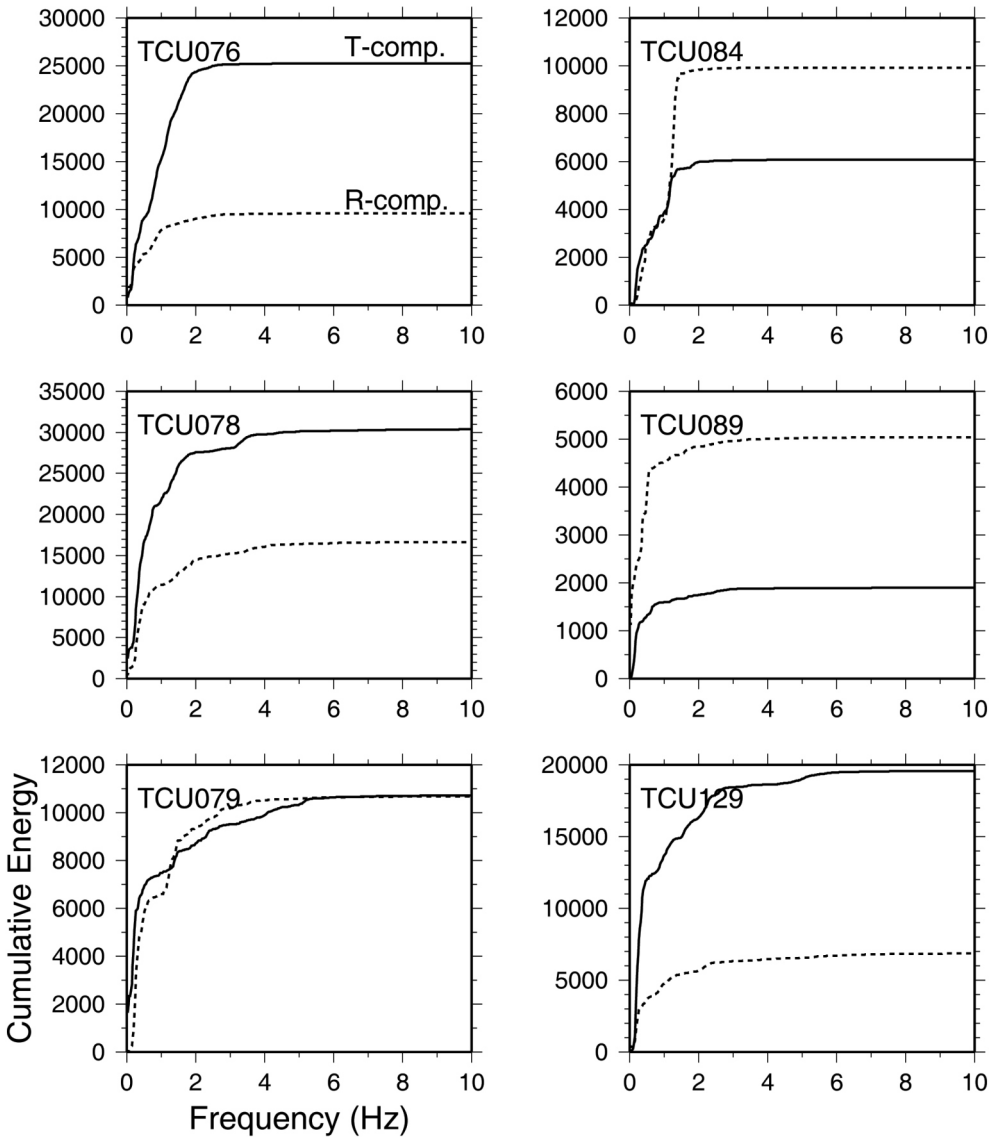

Fig. 3. Plots of cumulative energy versus frequency at 6 stations in use for the No. 2 event. The solid and dashed lines are for the *T*- and *R*-components, respectively.

$$D(f) = \quad /[1 \quad (f/f_c)^2] \tag{1}$$

The approximated Fourier spectral amplitude of velocity, $V(f)$ is:

$$V(f) = \quad f \quad /[1 \quad (f/f_c)^2] \tag{2}$$

In Eqs. (1) and (2), f_c is the corner frequency and is the spectral amplitude at the low-frequency spectral level. Andrews (1986) estimated the two parameters from seismograms using the following formulas: $= 2I_V^{0.75} / I_D^{0.25}$ and $f_c = (I_V / I_D)^{0.5} / 2$, where $I_V = V^2(f)df$ and $I_D = D^2(f)df$ are, respectively, the squared-velocity and squared-displacement integrals. In principle, the lower and upper bounds of integration are - and + , respectively. Equations (1) and (2) are applied to measure E_s and M_o by means of the following equations:

$$E_s = S_a \rho \beta I_V \tag{3}$$

and

$$M_o = 4 \quad r\rho\beta^3 \tag{4}$$

In Eqs. (3) and (4), ρ and β are, respectively, the density and the *S*-wave velocity of crustal materials in the study area. In this study, ρ = 2.8 g cm^{-3} and β = 3.5 km sec^{-1}. In Eq. (3), $S_a = 4 \quad r^2$ is the surface area of a sphere, centered with the hypocenter of an event, with a radius *r*, which is the hypocentral distance. It is noted that the terms to represent

the seismic radiation pattern are not included in the two formulas. Andrews' method for measuring E_s, i.e., Eq. (3), is essentially the same as others (Kikuchi and Fukao 1988; Singh and Ordaz 1994; Choy and Boatwright 1995; Pérez-Campos et al. 2003). However, there are some differences between the method, i.e., Eq. (4), for measuring M_o and others. This point will be discussed below.

We estimate and f_c directly from the predominant *S*-waves of the *T*- and *R*-component waveforms. The predominant *S*-waves of No. 2 Event at 6 seismic stations are depicted by two short dashed lines in the rotated displacement waveforms as shown in Fig. 2. The value of at a station is the averaged spectral amplitude at the low-frequency spectral level calculated from the two components, and the value of f_c is the average of those computed from all stations in use. Figure 4 shows the displacement spectra of No. 2 Event, at six stations. The solid lines denote the corrected spectra at 6 stations for No. 2 event, and the dashed lines display the source spectra based on the ω-squared model (Brune 1970) with various and an identical f_c. The observed displacement spectra of 6 stations show good fit with the theoretical source model. The amplitudes of the observed spectra decrease abruptly at $f > 6$ Hz. This is due to band-pass filtration of seismograms and high-cut filtration at high frequencies as mentioned above. Obviously, the amplitudes decay with f almost in a form of f^{-2} when $f > f_c$. The estimated values of f_c for the 22 events are in the range of 0.15 - 1.3 Hz, which are listed in Table 1.

The terms to represent the seismic radiation term are not included in Eqs. (3) and (4). Because of an incomplete azi-

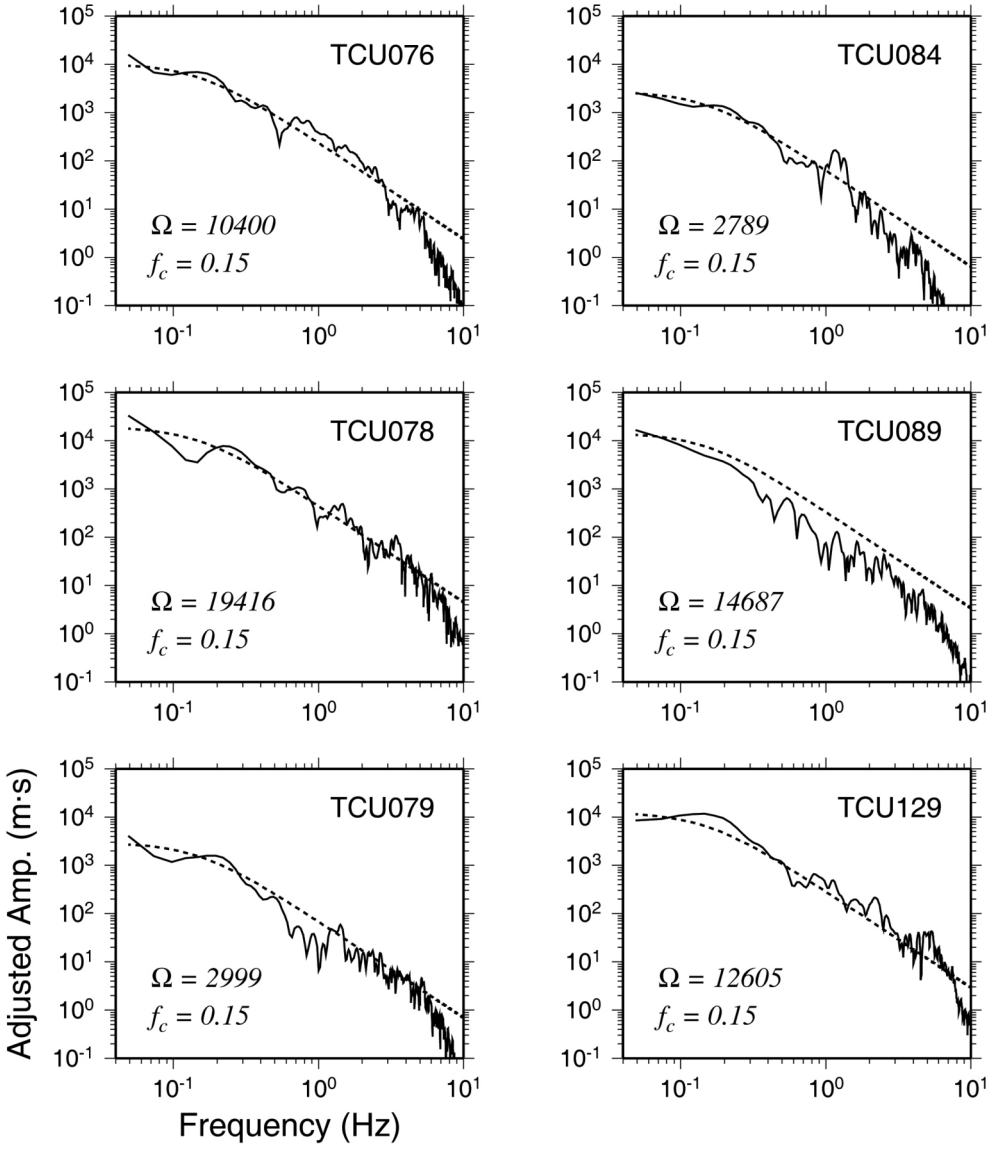

Fig. 4. The adjusted source spectra of 6 stations for the No. 2 event. The solid line is the record. The dashed line represents the spectra based on ω-squared model. The f_c is the averaged corner frequency of each station. The is the low-frequency spectral level.

muthal coverage of seismic stations and an absence of focal mechanisms of 8 events, an average radiation pattern with a value of 0.63 for the *S*-waves is adopted to adjust the amount of seismic energy caused by a non-uniform spatial distribution of seismic-wave radiation pattern (cf. Aki and Richards 1980; Boore and Boatwright 1984). In order to include the free-surface amplification, the seismograms are corrected by a factor of 2. In addition, a lack of a detailed spatial distribution of *Q*-value in the study area makes us unable to consider non-uniform seismic attenuation. Only frequency-independent Q_s for the *S*-waves, i.e., $Q_s = 250$, obtained by Rau et al. (1996) for central Taiwan is used to correct the waveforms.

4. SITE EFFECT AND FINITE FREQUENCY BANDWIDTH LIMITATION

The value of E_s could be improperly estimated from local seismograms due to site effect as pointed out by several authors (Boatwright et al. 2002; Pérez-Campos et al. 2003). The effect could be very large when the seismic station is situated at a soil site. According to Boore and Joyner (1997), site amplification varies from 1 to 2.58 when f increases from 0.01 to 6.05 Hz for generic rock sites, with an average shear velocity of 620 m sec^{-1}, and from 1 to 1.15 when f increases from 0.01 to 8 Hz for generic very hard rock sites, with an average shear velocity of 2900 m sec^{-1}. It is obvious that site amplification could be large at a soil site and very small at a very hard rock site.

Huang et al. (2005) investigated frequency-dependent site amplifications for about $f > 1$ Hz based on the well-logging data (to 30 m) at 87 station sites in central Taiwan. Huang (2006) and Huang et al. (2007) re-constructed the velocity and density model to evaluate frequency-dependent site amplifications for $f > 0.01$ Hz. According to site classifications of Huang et al. (2005), most of the stations in use for the 22 aftershocks are catalogued to Class-C and D sites, only a few of them are Class-E sites. For a detailed description concerning frequency-dependent site amplifications see Huang et al. (2005), Huang (2006), and Huang et al. (2007). Only the average site amplifications for the three kinds of sites at several discrete frequencies are given in Table 2. It is obvious from this table that site amplification increases with frequency. The site amplifications are the largest at Class-E sites, midrange at Class-D sites, and the smallest at Class-C sites.

It is noted that at some stations, the amplification function cannot be constructed due to a lack of a velocity model. An alternative way to construct a site amplification function at such stations is explained below: It is assumed that the amplification functions at two stations several kilometers apart are similar because the velocity model varies almost smoothly for a distance of 10 km (cf. Ma et al. 1996). Therefore, the amplification function at a nearby station is taken to be that of the station at which the amplification function cannot be constructed.

The site amplification functions constructed by Huang et al. (2005) and Huang (2006) did not include site attenuation, which makes spectral amplitudes decrease at high frequencies ($f > 1$ Hz). Anderson and Hough (1984) applied an exponential form of $e^{-\kappa f}$, where κ is a frequency-independent factor (in units of seconds), to represent the attenuation effect at shallow depths, especially for high frequencies. From the computation of Huang (2006), at a certain frequency the amplification decreases with increasing κ and the differences in amplification functions between various κ, i.e., 0.03, 0.04, and 0.05 sec, is small. The largest amplifications with $\kappa = 0.03$ sec is about 20% higher than those with $\kappa = 0.05$ sec when $f < 6$ Hz. In this study, we consider $\kappa = 0.03$ sec for high-frequency filtration.

In addition to the factors mentioned previously, seismograms are also affected by finite frequency bandwidth limitation due to instrumental response or filtration (Wang 2004). In principal, all source parameters are measured in the whole frequency range of 0 - Hz. But, in practice the measurement can be performed only in a frequency range of f_l - f_u, with $f_l < f_c < f_u$, where f_l and f_u are the low-bound and high-bound frequency, respectively. Hence, finite frequency bandwidth limitation must be taken into account. For details on how to eliminate this effect see Wang (2004) and Huang (2006); a simple description is given below.

Table 2. The values of site amplifications, $A(f)$, in the frequency range 0.01 - 2 Hz for Class-C, D, and E sites evaluated from the velocity structures constructed from well-loggings data and velocity models inferred from earthquake data in central Taiwan.

Frequency (Hz)	Classification		
	C	D	E
0.01	1.00	1.00	1.00
0.09	1.22	1.41	1.48
0.16	1.41	1.81	1.97
0.51	1.99	3.25	3.68
0.84	2.29	3.96	4.56
1.25	2.53	4.47	5.23
2.26	2.90	4.83	5.75
3.17	3.09	4.95	5.93
6.05	3.29	5.16	6.26
10.0	3.43	5.32	6.49
16.6	3.55	5.45	6.67
21.0	3.61	5.50	6.75

Inserting Eq. (1) into the integral of I_D leads to:

$$I_D = 2\Omega^2 \int \left[1 + \left(\frac{f}{f_c}\right)^2\right]^{-2} df \quad (5)$$

where the integral range is from f_l to f_u. In principle, can be exactly and independently determined from the low-frequency level of source spectra, and, thus, it is regarded as a constant. Thus, Eq. (5) becomes:

$$I_D = \Omega^2 f_c \left[\frac{f_{uc}}{1 + f_{uc}^2} - \frac{f_{lc}}{1 + f_{lc}^2} + \tan^{-1}(f_{uc}) - \tan^{-1}(f_{lc})\right] \quad (6)$$

where f_{uc} $\frac{f_u}{f_c}$ and f_{lc} $\frac{f_l}{f_c}$.

Define $I_D = I_{Do} F_D$, where,

$$I_{Do} = \frac{\Omega^2 2\pi f_c}{4} \quad (7)$$

and

$$F_D = \frac{2}{\pi}\left[\frac{f_{uc}}{1 + f_{uc}^2} - \frac{f_{lc}}{1 + f_{lc}^2} + \tan^{-1}(f_{uc}) - \tan^{-1}(f_{lc})\right] \quad (8)$$

Similarly, inserting Eq. (2) into the integral of I_V gives:

$$I_V = 2\Omega^2 \int (2\pi f)^2 \left[1 + \left(\frac{f}{f_c}\right)^2\right]^{-2} df \quad (9)$$

where the integral range is from f_l to f_u. After integration, Eq. (9) becomes:

$$I_V = \Omega^2 4\pi^2 f_c^3 \left[-\frac{f_{uc}}{1 + f_{uc}^2} + \frac{f_{lc}}{1 + f_{lc}^2} + \tan^{-1}(f_{uc}) - \tan^{-1}(f_{lc})\right] \quad (10)$$

Define $I_V = I_{Vo} F_V$, where,

$$I_{Vo} = \Omega^2 \frac{(2\pi f_c)^3}{4} \quad (11)$$

and

$$F_V = \frac{2}{\pi}\left[\frac{-f_{uc}}{1 + f_{uc}^2} + \frac{f_{lc}}{1 + f_{lc}^2} + \tan^{-1}(f_{uc}) - \tan^{-1}(f_{lc})\right] \quad (12)$$

Equations (3), (4), (8), and (12) lead to:

$$E_s = E_{s0} F_V \quad (13)$$

and

$$M_o = M_{o0} \frac{F_D^{0.75}}{F_V^{0.25}} \quad (14)$$

In Eqs. (13) and (14), the two source parameters without finite frequency bandwidth limitation are:

$$E_{s0} = S_a \rho \beta I_{V0} \quad (15)$$

and

$$M_{o0} = 4\pi r \rho \beta^3 \left(2\frac{I_{D0}^{0.75}}{I_{V0}^{0.25}}\right) \quad (16)$$

Obviously, F_V and F_D are functions of f_c, f_l, and f_u. By way of example, according to Eqs. (3) and (4), corrections for the measurement of E_s and M_o are given utilizing the following settings: f_c varies in the frequency band 0.25 - 2.2 Hz when f_l = 0.05 Hz and f_u = 6 Hz:

(1) For E_s: From Eq. (13), the variation of E_s/E_{s0} with f_c is shown by a solid line in Fig. 5. Obviously $E_s/E_{s0} < 1$ and E_s/E_{s0} gradually decrease with increasing f_c. E_s would be underestimated over the finite frequency band.
(2) For M_o: From Eq. (14), the variation of M_o/M_{o0} with f_c is shown by a dashed line in Fig. 5. It is obvious that M_o/M_{o0} monotonously increases with f_c and its value is less than 1 when f_c 1 Hz and larger than 1 when $f_c > 1$ Hz. This suggests that M_o would be underestimated when $f_c < 1$ Hz, yet overestimated M_o when $f_c > 1$ Hz.
(3) For $(E_s/E_{s0})/(M_o/M_{o0})$: From Eqs. (15) and (16), the variation of $(E_s/E_{s0})/(M_o/M_{o0})$ with f_c is shown by a dotted line in Fig. 5. It is obvious that $(E_s/E_{s0})/(M_o/M_{o0})$ decreases monotonously with increasing f_c. The value of $(E_s/E_{s0})/(M_o/M_{o0})$ is larger than 1 when $f_c < 0.4$ Hz and less than 1 when $f_c > 0.4$ Hz.

5. RESULTS

The ratios of E_s and M_o with the corrections for site am-

plification and finite frequency bandwidth limitation to those without corrections are shown, respectively, in Figs. 6a and b. The open squares are used for the ratios with only the correction for site effect and the solid squares for those with both corrections. Comparison between the seismic radiation energy estimated from local seismograms and that from teleseismic data is shown in Fig. 7. The values of E_s of ten events listed in the Harvard CMT catalogue are calculated from the Gutenberg-Richter's energy-magnitude law (abbreviated as the *GR* law hereafter) (Gutenberg and Richter 1955) and denoted as E_{sGR}. The bisection line is displayed by a solid line. Almost all data points are below the bisection line, thus indicating that $E_{sGR} < E_s$. Hence, the seismic radiation energy estimated from teleseismic data is smaller than that evaluated from local seismograms. The difference between E_s and E_{sGR} varies in a larger range for large earthquakes ($E_s > 10^{22}$ g cm^2 sec^{-2}) than for small events ($E_s < 10^{22}$ g cm^2 sec^{-2}).

Andrews' method of measuring M_o is different from others. In order to explore the feasibility of using this method to measure M_o from local seismograms, the values of M_{oH}, which were estimated from the teleseismic data of ten events, listed in the Harvard CMT catalogue, and those denoted by M_o of this study are compared. The log-log plot of M_{oH} versus M_o for the ten events is shown as open squares in Fig. 8. The values of M_{oB} from the catalogue of the Broadband Array in Taiwan for Seismology (BATS) for 14 events and those of this study are shown as solid squares in Fig. 8. (The BATS is operated by the Institute of Earth Sciences, Academia Sinica and the details about the array can be found on the website: http://bats.earth.sinica.edu.tw/.) In Fig. 8, the bisection line is displayed by a solid line. In general, both M_{oH} and M_{oB} are smaller than M_o. On average, $M_{oH} = 0.5\ M_o$ and $M_{oB} = 0.3\ M_o$. However, the difference between M_o and M_{oH} as well as M_{oB} is smaller for large M_o than for small M_o. In addition, M_{oH} is larger than M_{oB}. However, Fig. 8 confirms the feasibility of using Andrews' method to measure M_o from local seismograms, especially for larger-sized events. Of course, this method leads to slight overestimates of M_o for smaller-sized events.

Table 1 shows $E_s = 2.0 \quad 10^{18} - 8.9 \quad 10^{21}$ g cm^2 sec^{-2} and $M_o = 1.3 \quad 10^{23} - 1.4 \quad 10^{26}$ g cm sec^{-2} cm^{-1}. This gives $E_s/M_o = 7.4 \quad 10^{-6} - 2.6 \quad 10^{-4}$, with an average of ~7.9 $\quad 10^{-5}$. Although E_s is slightly under-estimated, the values of E_s/M_o are still in the range of those measured from both *P*- and *S*-waves by several authors as mentioned in "Introduction." Hence, the error caused by under-estimate could be low. Figure 9 shows the log-log plot of E_s versus M_o in the solid squares, with one-standard-deviation bars, for the 22 events. Hwang et al. (2001) measured the values of E_s (= 3.6 10^{23} g cm^2 sec^{-2}) and M_o (= 1.96 $\quad 10^{27}$ g cm sec^{-2} cm^{-1}) of the Chi-Chi mainshock from near-fault seismic data. Wang (2004) re-evaluated their value of E_s by removing finite frequency bandwidth limitation and the revised value is E_s = 4.3 10^{23} g cm^2 sec^{-2}. Here, the value of M_o is corrected by remov-

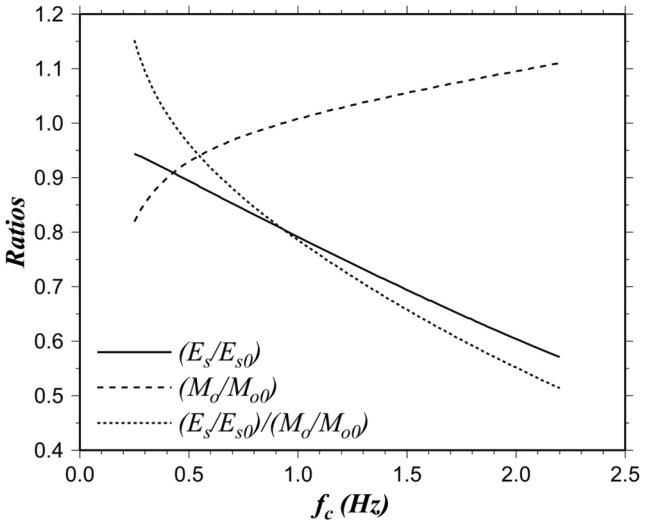

Fig. 5. The effects of the finite frequency bandwidth limitation on E_s, M_o, and scaled energy with various f_c, when $f_l = 0.05$ Hz and $f_u = 6$ Hz.

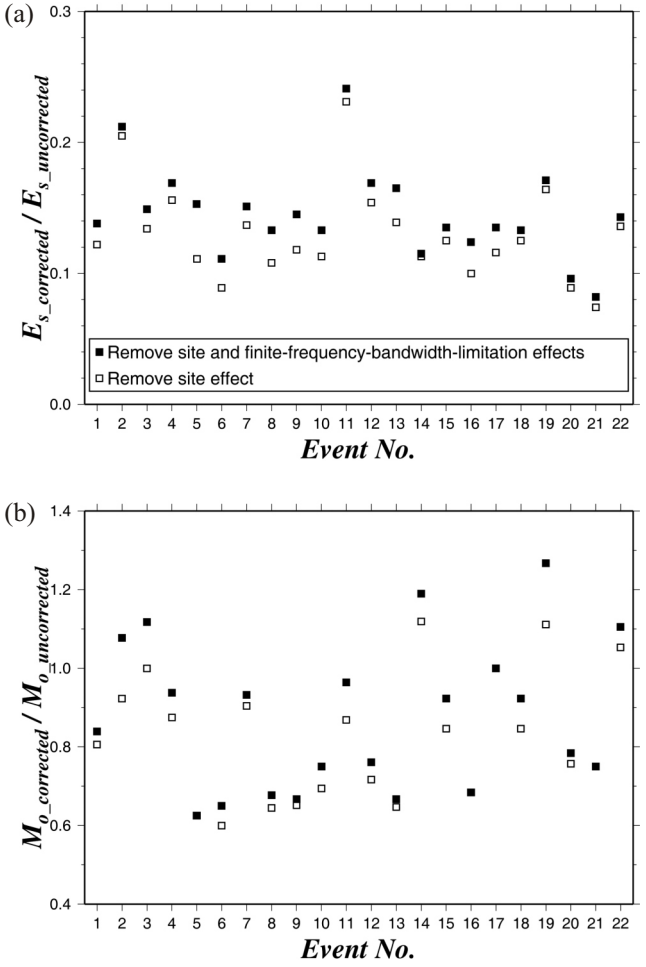

Fig. 6. (a) The ratio of E_s with corrections (i.e., site effect and finite-frequency-band limitation) to that without corrections for 22 events. (b) The ratio of M_o with corrections to that without corrections for 22 events. The open symbols represent that points only remove the site effect. Points removing both effects are denoted by solid symbols.

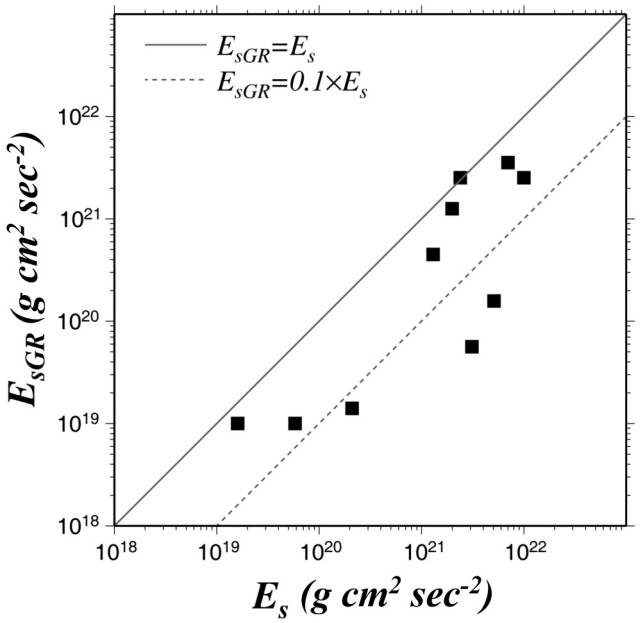

Fig. 7. The log-log plot of E_{sGR} versus E_s: E_{sGR} estimated from the Gutenberg-Richter's energy-magnitude law for ten events listed in the Harvard CMT catalogue. The solid line denotes the bisection line.

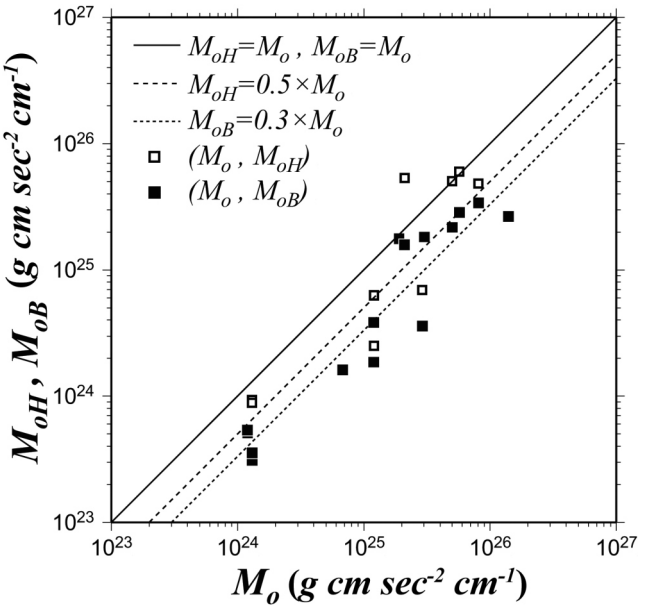

Fig. 8. The log-log plot of M_{oH} and M_{oB} versus M_o. M_{oH} obtained from the Harvard CMT catalogue, and M_{oB} obtained from the BATS catalogue. The solid line denotes the bisection line.

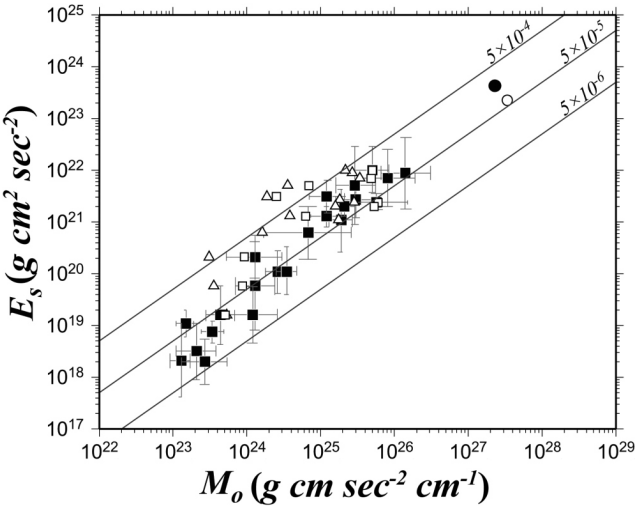

Fig. 9. The log-log plot of E_s versus M_o. The three lines are associated with three values of E_s/M_o, i.e., 5 10^{-4}, 5 10^{-5}, and 5 10^{-6}. (Symbols: the solid squares for the values of E_s and M_o of 22 aftershocks measured from local data, the open squares for E_s of this study and M_o listed in the Harvard CMT catalogue, the open triangles for E_s of this study and M_o listed in the BATS catalogue, the solid circle for that of the mainshock measured from four near-fault seismograms by Hwang et al. (2001), and the open circle for that of the mainshock obtained from the Harvard CMT catalogue).

ing finite frequency bandwidth limitation and the revised value is M_o = 2.3 10^{27} g cm sec^{-2} cm^{-1}. In Fig. 9, a solid circle denotes the data points of the Chi-Chi mainshock. Included also in Fig. 9 are the data points (in open squares) for both aftershocks and the mainshock with M_{oH} and E_s of this study, and the open triangles for those with M_{oB} and E_s of this study.

In order to study the correlation of E_s/M_o versus M_s, it is necessary to have the values of M_s for all events. Since the values of M_s of ten events are not given in the Harvard CMT catalogue, we estimate the values from their local magnitudes, M_L. The plot of M_L versus M_s for the 10 events, whose values of M_L and M_s are listed, respectively, in the CWB catalogue and in the Harvard CMT catalogue, is shown in Fig. 10. There is a linear regression relationship between the two magnitude scales: M_s = 1.14 M_L – 1.41 0.30, with a high correlation coefficient of 0.90. Hence, the values of M_s of remaining twelve aftershocks without M_s can be estimated directly from this relationship (M_s in parentheses in Table 1). Figure 11 shows the plot of E_s/M_o versus M_s: solid squares for both E_s and M_o of this study, open squares for E_s of this study and M_{oH}, and open triangles for E_s of this study and M_{oB}. For the purpose of comparison, included also are the data points for the Chi-Chi mainshock. The values of E_s/M_o evaluated in this study are in the range 4.2 10^{-5} – 2.6 10^{-4} when M_s > 5, and in the range 7.4 10^{-6} – 1.6 10^{-4} when M_s < 5. Since the measured value of E_s would be slightly smaller than the real one as mentioned above, the value of E_s/M_o should be slightly less than the real one.

6. DISCUSSION

Taking a constant value of Q_s to correct attenuation of

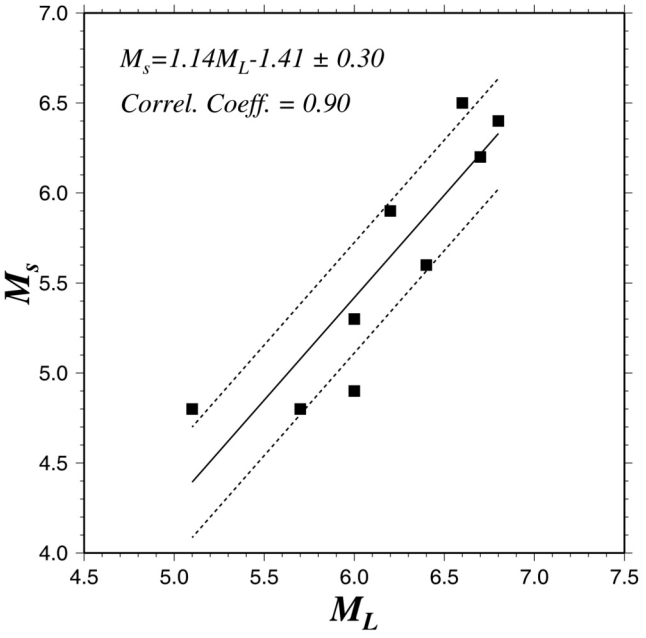

Fig. 10. Plots of M_s versus M_L. The M_s values are from the Harvard CMT catalogue, while the M_L values are from the CWB catalogue.

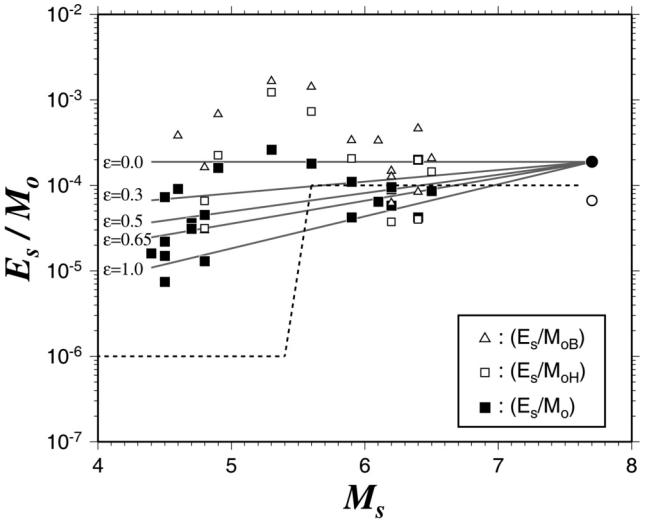

Fig. 11. The plot of log(E_s/M_o) versus M_s: solid symbols for this study and open symbols for the results obtained from the Harvard CMT catalogue. Squares are for aftershocks and circles are for mainshock. The solid lines show the relationship proposed by Kanamori and Rivera (2004), while the dashed line is proposed by Brodsky and Kanamori (2001).

seismic waves could lead to deviation on estimation of f_c, which is affected by variations in spectral amplitudes on the basis of Andrews' method. As shown in Table 1, the values of f_c vary in the range of 0.15 - 1.3 Hz. In order to test the effect due to a change of Q_s on spectral amplitudes, three values of Q_s, i.e., 200, 250, and 300, are taken into account. The spectra amplitudes with f = 1.3 Hz at an epicentral distance of 50 km are 75%, 79%, and 86%, respectively. The percentage error is smaller than 7%. Since the epicentral distance in use is less than 50 km, the effect due to a change of Q_s on f_c would be small and can be ignored.

Figure 5 shows that finite frequency bandwidth limitation actually results in remarkable influence on the measures of E_s, M_o, and E_s/M_o. From Eq. (15), the variation of E_s/E_{s0} with f_c is shown in Fig. 5 (solid line). Finite frequency bandwidth limitation leads to an underestimation of E_s, and such an underestimation increases with f_c. In other words, the underestimation is greater for a smaller event with larger f_c than for a larger event with smaller f_c. This is consistent with the point stressed by several authors (Boore 1988; Di Bona and Rovelli 1988; Singh and Ordaz 1994; Wang 2004). From Eq. (16), the variation of M_o/M_{o0} with f_c is shown in Fig. 5 (dashed line). Obviously, finite frequency bandwidth limitation leads to an underestimation of M_o at $f_c < 0.9$ Hz, and an increase monotonously overestimates M_o at $f_c > 0.9$ Hz. In other words, underestimation occurs for a larger event with smaller f_c; however, overestimation occurs for a smaller event with larger f_c. It is obvious that M_o M_{o0} when f_c 0.9 Hz.

From Eqs. (15) and (16), the variation of $(E_s/M_o)/(E_{s0}/M_{o0})$ with f_c is shown in Fig. 5 (dotted line). It is obvious that $(E_s/M_o)/(E_{s0}/M_{o0})$ monotonously decreases with increasing f_c. The value of $(E_s/M_o)/(E_{s0}/M_{o0})$ is larger than 1 when $f_c < 0.4$ Hz and less than 1 when $f_c > 0.4$ Hz. This variation is mainly due to a monotonous increase in M_o/M_{o0} with f_c and small variation of E_s with f_c. Results obviously show that finite frequency bandwidth limitation leads to an overestimate of scaled energy for larger events with $f_c < 0.4$ Hz and an underestimate for smaller events with $f_c > 0.4$ Hz.

Figure 6 shows that after removing the site effect, the ratio for E_s ranges from 0.07 to 0.23. Obviously, E_s is overestimated for all the events when the site effect is included. For No. 21 event, the ratio is the smallest due to the largest site amplification because the stations are located on the Western Plain, which has thick sediments (cf. Huang 2006). After correcting finite frequency bandwidth limitation, the ratio of E_s only slightly increases. This means that finite frequency bandwidth limitation yields a smaller effect on estimates of E_s than site amplification. After removing the site effect, the ratio for M_o ranges from 0.6 to 1.15. The value of M_o is overestimated by a factor of 0.4 for most events and underestimated by a factor of 0.15 for few events, i.e., Nos. 2, 3, 14, 19, and 22. This suggests that site amplification makes a smaller effect on M_o than on E_s, because M_o is evaluated mainly from lower-frequency signals with a lower site effect. Figure 6b shows that except for few events finite frequency bandwidth limitation also results in a small effect on M_o.

In Fig. 9, the solid lines are associated, respectively, with three values of E_s/M_o, i.e., 5 10^{-4}, 5 10^{-5}, and 5 10^{-6}, calculated from the E_s-M_o relationship obtained from

global observations (Vassiliou and Kanamori 1982; Kikuchi and Fukao 1988). The data points of the 22 events distribute almost around the line with $E_s/M_o = 5$ 10^{-5}. The data points of E_s/M_o for M_o obtained from local seismograms and those for M_o from teleseismic data mix together when $M_o > 10^{25}$ g cm sec^{-2} cm^{-1}. The data points for local seismic data are below those for M_o from teleseismic data. This indicates that the values of E_s/M_o for M_o obtained from local seismograms are somewhat smaller than those for M_o from teleseismic data when $M_o < 10^{25}$ g cm sec^{-2} cm^{-1}. On the other hand, Smith et al. (1991), Singh and Ordas (1994), and Hwang et al. (2001) had an opposite conclusion. Different frequency bands and different frequency bandwidths would both lead to different measured values of E_s and M_o whether the measures are made from local seismograms or from teleseismic data. However, there is a problem for teleseismic data. Usually, the high-frequency signals, which are strong in local seismograms, become weak in teleseismic data because of high attenuation on the high-frequency signals. This will affect the measure of E_s from teleseismic data. Boore (1988), Di Bona and Rovelli (1988), Singh and Ordaz (1994), and Wang (2004) stressed that E_s can be severely underestimated when high-frequency signals are not used. Hence, E_s estimated from local seismograms can be higher than that from teleseismic data. Since, the values of E_s in this study are measured from local seismograms, the difference in E_s/M_o between local and teleseimic data must be due to the method of measuring M_o. For local data, M_o is measured from higher-frequency signals. From Fig. 5, it is obvious that the values of M_o are underestimated from local data when $f_c = 0.15 – 1.30$ Hz. For teleseismic data, M_o is measured from lower-frequency signals. The value of M_o in the Harvard CMT catalogue is routinely measured from the 300-second waves and that in the BATS catalogue from the 20-second waves. Higher-frequency signals are stronger in local seismograms than in teleseismic data. This yields that M_o is either overestimated from local seismograms using Andrews' method or underestimated from teleseismic data. Lower-frequency signals are weaker for smaller-sized earthquakes than for larger-sized events. Hence, M_o can be underestimated for smaller-sized events from teleseismic data.

In Fig. 11, a small number of data points make us unable to obtain a simple relationship between E_s/M_o and M_s. Nevertheless, a correlation between the two quantities can be seen from the plot. It is obvious that E_s/M_o is, on average, smaller for $M_s < 5$ than for $M_s > 5$, and thus, E_s/M_o increases with M_s. On the other hand, except for the two events with $M_s = 5.3$ and 5.6, E_s/M_o with M_o from either the Harvard CMT catalogue or the BATS catalogue does not depend on M_s. Ide and Beroza (2001) stated that E_s/M_o does not depend on seismic-moment magnitude, M_w, which is the same as M_s, over a large range of M_w from -4 to +9. On the contrary, Brodsky and Kanamori (2001) reported an abrupt change of E_s/M_o from 10^{-6} to 10^{-4} in a narrow range around $M_s = 5.5$ (shown by a dashed line in Fig. 11) and applied the elasto-hydrodynamic lubrication model to interpret such a marked change. However, the data points of this study agree with the dashed line when $M_s > 5.5$, but are above the dashed line when $M_s < 5.5$. No marked change of E_s/M_o with M_s in the whole magnitude range can be delineated. For the purpose of comparison, included also in Fig. 11 are ten data points in open squares with M_o shown in the Harvard CMT catalogue and 14 data points in open triangles with M_o listed in the BATS catalogue. The two kinds of data points are all above and cannot be described by the line as suggested by Brodsky and Kanamori (2001).

From a theoretical analysis, Kanamori and Rivera (2004) stated that the $M_o \sim f_c^{-3}$ scaling relation leads to independence of E_s/M_o on earthquake magnitude. They claimed that when the M_o versus f_c scaling is modified from $M_o \sim f_c^{-3}$ to $M_o \sim f_c^{-(3+\varepsilon)}$, where $0 < \varepsilon$ 1, the scaled energy can be a function of earthquake magnitude, and stressed that $\varepsilon = 0.5$ is the optimum value. In order to understand the M_o-f_c scaling, the log-log plot of M_o versus f_c of the 22 aftershocks is shown with solid squares in Fig. 12. It is obvious that the linear regression equation between the two parameters is $\log(M_o) = -3.65\log(f_c) + 23.36$ 0.28, with a correlation coefficient of -0.94, thus leading to $\varepsilon = 0.65$. This gives a scaling law of $M_o \sim f_c^{-3.65}$. The M_o-f_c scaling for ten events of M_{oH} from the Harvard CMT catalogue and f_c in this study is shown with open squares in Fig. 12, which displays a linear regression

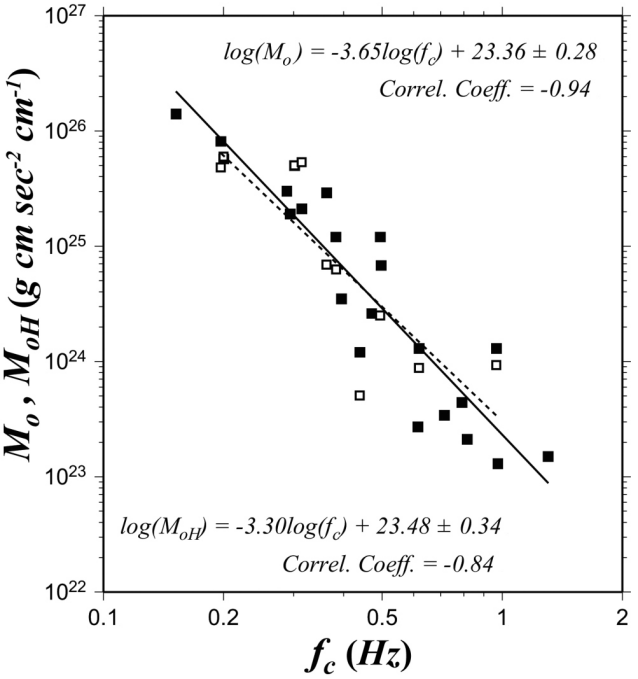

Fig. 12. The log-log plots of M_o versus f_c of the 22 events are denoted by solid squares; meanwhile, the log-log plots of M_{oH} from the Harvard CMT catalogue versus f_c of the 10 events are displayed with open squares. The solid line shows the linear regression equation for pairs of (M_o, f_c) and the dashed lines for pairs of (M_{oH}, f_c).

equation: $\log(M_{oH}) = -3.30\log(f_c) + 23.48 \quad 0.34$, with a correlation coefficient of -0.84, thus giving $\varepsilon = 0.3$.

According to variational calculus, Kanamori and Rivera (2004) calculate the minimum of E_s/M_o to the moment magnitude, M_w, by the following expression:

$$\log\left[\frac{\tilde{e}_{\min}(M_w)}{\tilde{e}_{\min}(M_{w0})}\right] = 1.5(M_w - M_{w0})\frac{\varepsilon}{(3+\varepsilon)} \qquad (17)$$

where $\tilde{e}_{\min}(M_w)$ and $\tilde{e}_{\min}(M_{w0})$ are the minima of E_s/M_o at M_w and a reference magnitude M_{w0}. The reference magnitude M_{s0} or M_{w0} is 7.7 in this study. Five solid lines associated with $\varepsilon = 0$, 0.3, 0.5, 0.65, and 1 are displayed in Fig. 11. When the two data points with $M_s = 5.3$ and 5.6 are not included, the distribution of solid squares seems able to be described by the dashed lines with $\varepsilon = 0.5$ or 0.65, in other words, E_s/M_o increases with M_s. This means that the concept proposed by Kanamori and Rivera (2004) is acceptable. On average, the distributions of data points denoted by triangles and open squares can be interpreted by the dashed line with $\varepsilon = 0$, in other words, E_s/M_o is independent of M_s. Like Ide and Beroza (2001), this indicates that the concept proposed by Kanamori and Rivera (2004) is not acceptable. The difference between the two distributions of data points is mainly due to the way of evaluating M_o, because E_s is the same for the two distributions. As mentioned above, the value of M_o evaluated from local seismograms is, on average, 2 times larger than that done from teleseismic data, especially for smaller-sized events. This reduces the value of E_s/M_o for smaller-sized events. After correcting this reduction, E_s/M_o should be independent of M_s.

Figure 13 shows the depth distribution of $\ln(E_s/M_o)$. The solid squares represent the results for M_o evaluated in this study. Included also is the result of Chi-Chi mainshock. A regression relationship of E_s/M_o versus depth is constructed:

$$\ln(E_s/M_o) = 0.09 \quad h - 10.86 \quad 0.75 \qquad (18)$$

where h is the focal depth in km. The correlation coefficient of Eq. (18) is 0.57, that is, $\ln(E_s/M_o)$ is correlated with depth in a lower degree. The slop of Eq. (18) is 0.09, and, thus, suggests that $\ln(E_s/M_o)$ only slightly increase with depth. Since larger-sized earthquakes are generally recorded by a larger number of seismic stations, the error of the inferred focal depth is less than 5 km (cf. CWB 2003). It is noted that the data points (denoted by a solid circle) associated with the two subevents of the mainshock also follow the trend. This implicates that the depth variation of E_s/M_o can show overall behavior of the whole source area, because the aftershocks in use are located to the east of the Chelungpu fault. Equation (18) leads to $E_s/M_o = 1.92 \quad 10^{-5}e^{0.09h}$, thus indicating that the energy radiated per unit seismic moment slightly increases exponentially with depth. This is inconsistent with the result obtained by Vassiliou and Kanamori (1982) that the value of E_s/M_o is larger for shallow earthquakes than for deep and intermediate events. Of course, the events used in this study can only be classified as the shallow ones of theirs. Several factors, including geo-temperature, lithostatic pressure, crustal composition etc., would influence the depth variation of E_s/M_o. Equation (18) leads to the depth variation of the apparent stress, i.e., $\sigma_a = \mu(E_s/M_o)$, where μ = rigidity, in the following form: $\sigma_a = 3.3 \quad 10^9 \quad (1.92 \quad 10^{-5}e^{0.09h}) = 6.3 \quad 10^4 e^{0.09h}$ (σ_a in kg-m sec^{-2} m^{-2}), or $_a = 6.3 \quad 10^4 e^{0.09h}$ (in kg-m sec^{-2} m^{-2}). As $h < 10$ km, the exponential form can be approximated by a linear one: $\sigma_a = 6.3 \quad 10^4 + 5.7 \quad 10^3 h$ (in kg-m sec^{-2} m^{-2}), and, thus, the gradient of $_a$ in the upper crust is about 5.7 10^3 kg-m sec^{-2} m^{-2}-km. The average lithostatic pressure is $\sigma_o = \rho g h$ (in kg-m sec^{-2} m^{-2}), where $\rho = 2.75 \quad 10^3$ kg m^{-3}, and $g = 10$ m sec^{-2}. For example, the value of σ_a at $h = 8$ km is 1.1 10^6 kg-m sec^{-2} m^{-2}, which is about one-twentieth of average σ_o, i.e., σ_o, at this depth (about 2.2 10^7 kg-m sec^{-2} m^{-2}). McGarr (1999) stated $\sigma_a \quad 0.06\sigma_o$. Hence, this seems to show that the depth-dependence of E_s/M_o is acceptable.

7. CONCLUSIONS

Site amplification and finite frequency bandwidth limitation both influence the measures of scaled energy i.e., the ratio of seismic radiated energy to seismic moment, and the influence is larger for the former than for the latter. The values of E_s measured from the *S*-waves of local seismograms are larger than those calculated from the Gutenberg-Richter's energy-magnitude law. Of course, the difference is smaller for larger-sized events. As compared with the values of M_o of this study and those estimated from teleseismic

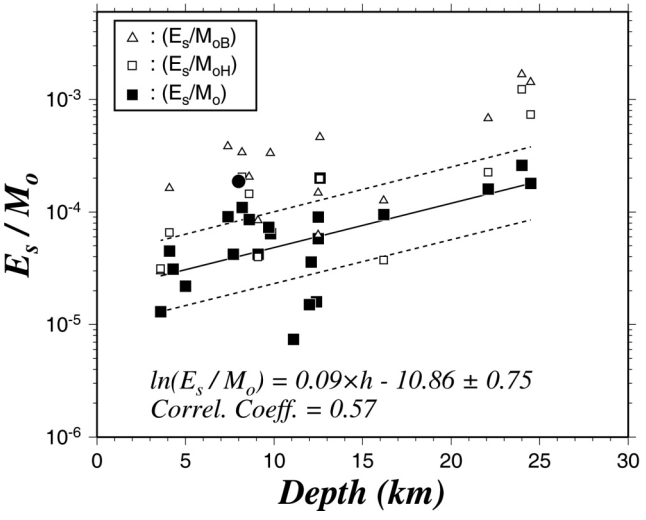

Fig. 13. The plot of $\ln(E_s/M_o)$ versus focal depth. The solid line shows the linear regression equation and the dashed lines display the standard deviations (Symbols are the same as those shown in Fig. 11).

data, it is feasible to use the Andrews' method to measure M_o from local seismograms. The values of M_o measured using Andrews' method are larger than those listed in the BATS and Harvard CMT catalogues. The difference is smaller for larger events than for smaller ones. This means that Andrews' method can work well for larger-sized earthquakes. The values of E_s and M_o measured from local seismograms for twenty-two M_L 5.1 aftershocks of the 1999 Chi-Chi earthquake are: $E_s = 2.0$ $10^{18} - 8.9$ 10^{21} g cm^2 sec^{-2} and $M_o = 1.3$ $10^{23} - 1.4$ 10^{26} g cm sec^{-2} cm^{-1}. Hence, the scaled energy $E_s/M_o = 7.4$ $10^{-6} - 2.6$ 10^{-4}, with an average of ~7.9 10^{-5}. The scaled energy measured from local seismograms is somewhat larger than that done from teleseismic data. Results also show that the scaled energies of the 22 aftershocks are slightly dependent upon earthquake magnitude when both E_s and M_o are evaluated from local seismograms, yet independent when M_o is estimated from teleseismic data. M_o correlates to corner frequency, f_c, in the following scaling relation: $M_o \sim f_c^{-3.65}$. In addition, the scaled energy slightly depends on the depth in the following form: $E_s/M_o = 1.92$ $10^{-5} e^{0.09h}$.

Acknowledgements The author thanks two anonymous reviewers for their useful comments to improve the paper. The authors also thank the Central Weather Bureau, Taiwan for providing high-quality earthquake data. This study was sponsored by Academia Sinica and the National Science Council (under Grants: No. NSC94-2119-M-001-011 and No. NSC96-2116-M-001-012-MY3).

REFERENCES

Aki, K., 1967: Scaling law of seismic spectrum. *J. Geophys. Res.*, **72**, 1217-1231, doi: 10.1029/JZ072i004p01217. [Link]

Aki, K. and P. G. Richards, 1980: Quantitative Seismology, W. H. Freeman and Co., San Francisco, California, 932 pp.

Anderson, J. and S. Hough, 1984: A model for the shape of the Fourier amplitude spectrum of acceleration at high frequencies. *Bull. Seismol. Soc. Am.*, **74**, 1968-1993.

Andrews, D. J., 1986: Objective determination of source parameters and similarity of earthquakes of different size. In: Das, S., J. Boatwright, and C. H. Scholz (Eds.), Earthquake Source Mechanics, AGU, Washington, DC, 259-267.

Boatwright, J., G. L. Choy, and L. C. Seekins, 2002: Regional estimates of radiated seismic energy. *Bull. Seismol. Soc. Am.*, **92**, 1241-1255, doi: 10.1785/0120000932. [Link]

Bolt, B. A., 1986: Seismic Energy release over a broad frequency band. *Pure Appl. Geophys.*, **124**, 919-930, doi: 10.1007/BF00879618. [Link]

Boore, D. M., 1988: The effect of finite bandwidth on seismic scaling relationships. In: Scholz, C. H. (Ed.), Earthquake Source Mechanics, AGU Geophys. Mono., 27, 275-283, AGU, Washington, DC.

Boore, D. M. and J. Boatwright, 1984: Average body-wave radiation coefficients. *Bull. Seismol. Soc. Am.*, **74**, 1615-1621.

Boore, D. M. and W. B. Joyner, 1997: Site amplifications for generic rock sites. *Bull. Seismol. Soc. Am.*, **87**, 327-341.

Brodsky, E. E. and H. Kanamori, 2001: Elastohydrodynamic lubrication of faults. *J. Geophys. Res.*, **106**, 16357-16374, doi: 10.1029/2001JB000430. [Link]

Brune, J. N., 1970: Tectonic stress and the spectra of seismic shear waves from earthquakes. *J. Geophys. Res.*, **75**, 4997-5009, doi: 10.1029/JB075i026p04997. [Link]

Choy, G. L. and J. L. Boatwright, 1995: Global patterns of radiated seismic energy and apparent stress. *J. Geophys. Res.*, **100**, 18205-18228, doi: 10.1029/95JB01969. [Link]

CWB, *Seismological Bulletin, July to September 2003*, **50**, Central Weather Bureau, 141 pp.

Di Bona, M. and A. Rovelli, 1988: Effects of the bandwidth limitation on stress drops estimated from integrals of the ground motions. *Bull. Seismol. Soc. Am.*, **78**, 1818-1825.

Gutenberg, B. and C. F. Richter, 1955: Magnitude and energy of earthquakes. *Nature*, **176**, 795, doi: 10.1038/176795a0. [Link]

Huang, M. W., 2006: Estimates of seismic radiated energies and seismic moments of the aftershocks of 1999 Chi-Chi, Taiwan, earthquake using strong-motion data. Ph.D. Dissertation, National Central University, Taiwan, ROC, 157 pp.

Huang, M. W., J. H. Wang, R. D. Hwang, and K. C. Chen, 2002: Estimates of source parameters of two large aftershocks of the 1999 Chi-Chi, Taiwan, earthquake in Chia-Yi area. *Terr. Atmos. Ocean. Sci.*, **13**, 299-312.

Huang, M. W., J. H. Wang, H. H. Hsieh, K. L. Wen, and K. F. Ma, 2005: Frequency-dependent sites amplifications evaluated from well-logging data in central Taiwan. *Geophys. Res. Lett.*, **32**, L21302, doi: 10.1029/2005GL023527. [Link]

Huang, M. W., J. H. Wang, K. F. Ma, C. Y. Wang, J. H. Hung, and K. L. Wen, 2007: Frequency-dependent site amplifications with f 0.01 Hz evaluated from velocity and density models in central Taiwan. *Bull. Seismol. Soc. Am.*, **97**, 624-637, doi: 10.1785/0120060139. [Link]

Hwang, R. D., J. H. Wang, B. S. Huang, K. C. Chen, W. G. Huang, T. M. Chang, H. C. Chiu, and C. C. Tsai, 2001: Estimates of stress drop of the Chi-Chi, Taiwan, earthquake of 20 September 1999 from near-field seismograms. *Bull. Seismol. Soc. Am.*, **91**, 1158-1166, doi: 10.1785/0120000708. [Link]

Ide, S. and G. C. Beroza, 2001: Does apparent stress vary with earthquake size? *Geophys. Res. Lett.*, **28**, 3349-3352, doi: 10.1029/2001GL013106. [Link]

Kanamori, H., 1977: The energy release in great earthquakes. *J. Geophys. Res.*, **82**, 2981-2987, doi: 10.1029/JB082i020p02981. [Link]

Kanamori, H. and L. Rivera, 2004: Static and dynamic scaling relations for earthquakes and their implications for rupture speed and stress drop. *Bull. Seismol. Soc. Am.*, **94**, 314-319, doi: 10.1785/0120030159. [Link]

Kao, H., Y. H. Liu, W. T. Liang, and W. P. Chen, 2002: Source parameters of regional earthquakes in Taiwan: 1999-2000

including the Ch-Chi earthquake sequence. *Terr. Atmos. Ocean. Sci*., **13**, 279-298.

Kikuchi, M. and Y. Fukao, 1988: Seismic wave energy inferred from long-period body wave inversion. *Bull. Seismol. Soc. Am*., **78**, 1707-1724.

Kinoshita, S. and M. Ohike, 2002: Scaling relations of earthquakes that occurred in the upper part of the Philippine Sea plate beneath the Kanto region, Japan, estimated by means of borehole recordings. *Bull. Seismol. Soc. Am*., **92**, 611-624, doi: 10.1785/0120010134. [Link]

Liu, K. S., T. C. Shin, and Y. B. Tsai, 1999: A free-field strong motion network in Taiwan: TSMIP. *Terr. Atmos. Ocean. Sci*., **10**, 337-396.

Ma, K. F., C. T. Lee, Y. B. Tsai, T. C. Shin, and J. Mori, 1999: The Chi-Chi, Taiwan earthquake: Large surface displacements on an inland thrust fault. *EOS Trans., AGU*, **80**, 605-611, doi: 10.1029/99EO00405. [Link]

Ma, K. F., J. H. Wang, and D. Zhao, 1996: Three-dimensional seismic velocity structure of the crust and uppermost mantle beneath Taiwan. *J. Phys. Earth*, **44**, 85-105.

McGarr, A., 1999: On relating apparent stress to the stress causing earthquake fault slip. *J. Geophys. Res*., **104**, 3003-3011, doi: 10.1029/1998JB900083. [Link]

Pérez-Campos, X., S. K. Singh, and G. C. Beroza, 2003: Reconciling teleseismic and regional estimates of seismic energy. *Bull. Seismol. Soc. Am*., **93**, 2123-2130, doi: 10.1785/0120020212. [Link]

Rau, R. J., F. T. Wu, and T. C. Shin, 1996: Regional network focal mechanism determination using 3D velocity model and SH/P amplitude ratio. *Bull. Seismol. Soc. Am*., **86**, 1270-1283.

Shin, T. C., K. W. Kuo, W. H. K. Lee, T. L. Teng, and Y. B. Tsai, 2000: A preliminary report on the 1999 Chi-Chi (Taiwan) earthquake. *Seismol. Res. Lett*., **71**, 24-30.

Singh, S. K. and M. Ordaz, 1994: Seismic energy release in Mexican subduction zone earthquakes. *Bull. Seismol. Soc. Am*., **84**, 1533-1550.

Smith, K. D., J. N. Brune, and K. F. Priestley, 1991: The seismic spectrum, radiated energy, and the Savage and Wood inequality for complex earthquakes. *Tectonophys*., **188**, 303-320, doi: 10.1016/0040-1951(91)90461-Z. [Link]

Vassiliou, M. S. and H. Kanamori, 1982: The energy release in earthquakes. *Bull. Seismol. Soc. Am*., **72**, 371-387.

Wang, J. H., 2004: The seismic efficiency of the 1999 Chi-Chi, Taiwan, earthquake. *Geophys. Res. Lett*., **31**, L10613, doi: 10.1029/2004GL019417. [Link]

Wang, J. H. and M. W. Huang, 2007: Effect of finite frequency bandwidth limitation on evaluations of seismic radiation energy of the 1999 Chi-Chi Earthquake. *Terr. Atmos. Ocean. Sci*., **18**, 567-576, doi: 10.3319/TAO.2007.18.3.567(T). [Link]